

Computational insights into the binding mechanism of antagonists with neuropeptide B/W receptor 1†

Cite this: *Mol. BioSyst.*, 2014,
10, 2236

Mahesh Chandra Patra,^{*ab} Jitendra Maharana,^{*bc} Budheswar Dehury^d and Sachinandan De^a

Neuropeptide B/W receptor 1 (NPBWR1), previously known as G-protein coupled receptor 7 (GPR7), is a class A G-protein coupled receptor implicated in the modulation of several neuroendocrine functions such as feeding behavior, energy homeostasis, epilepsy, and analgesia. In recent years, a few antagonists have been designed that bind to NPBWR1 with high affinity. However, the exact binding modes between the antagonists and the receptor are still unknown. Unraveling the key pharmacophoric features of the receptor will guide the development of novel compounds with increased potency for therapeutic use. Here, we studied the structural organization of NPBWR1 receptor and its antagonist binding modes through computational approaches. Based on the dynamics and energetic features of receptor–ligand interactions, we categorized the binding affinities of the antagonists for NPBWR1 and identified key residues responsible for ligand recognition by NPBWR1. Binding free energy calculations revealed that the residues Trp102^{ECL1}, Val113^{3,29}, Gln281^{ECL3}, and Ala274^{6,58} were crucial for ligand interaction. The results of our study will be useful to understand the structure–function relationship of NPBWR1 that may assist future drug discovery initiatives.

Received 3rd April 2014,
Accepted 6th June 2014

DOI: 10.1039/c4mb00214h

www.rsc.org/molecularbiosystems

Introduction

Neuropeptide B/W receptor 1 (NPBWR1) and NPBWR2 are two structurally related G-protein coupled receptors (GPCRs),¹ which have recently been deorphanized with the successive identification of their cognate ligands, neuropeptide W (NPW) and neuropeptide B (NPB).^{2,3} NPBWR1 and 2 share 70% nucleotide and 64% amino acid homology with each other and are closely related to opioid and somatostatin-like receptor genes of the human genome. These receptors along with their ligands are exclusively localized to the central nervous system (CNS)⁴ and they have been linked with the regulation of feeding behavior and energy homeostasis in humans and rodents.^{2,3} Recently, it was reported that NPBWR1 modulates feeding behavior and energy balance by inducing lipolysis and slowing down leptin secretion.^{5,6} NPBWR1 is such an important

modulator of energy metabolism that knocking it out from mice caused adult-onset obesity.^{3,7} Accordingly, NPBWR1 has emerged as an attractive, novel therapeutic target for anti-obesity drugs.

Interestingly, a higher expression of NPBWR1 in patients with acute inflammatory and immune-mediated neuropathies suggested the importance of this receptor in analgesic behavior and modulation of inflammatory neuropathies.⁸ This indicated a new potential therapeutic target for treating inflammatory pain. The NPBWR1-NPB system is also associated with the regulation of the neuroendocrine system, cognitive and effective reactions to stress and arousal, locomotor activity, and cardiovascular responses.⁹

Remarkably, NPW shows anti-epileptic effect similar to other anticonvulsants drugs. This is evident from a recent study showing intracerebroventricular (i.c.v) administration of NPW to the mice brain reduced epileptic seizure, suggesting that NPBWR1 is a potential anti-epileptic target of therapeutic importance.¹⁰

Until now, sufficient evidence has been obtained signifying that NPBWR1 is a key modulator of feeding behavior, energy homeostasis, neuroendocrine function, and inflammatory pain.¹¹ However, an accurate evaluation of ligand recognition and receptor activation is still not done, probably due to the absence of suitable pharmacological tools. Several groups have discovered, synthesized, and carried out structure–activity relationship (SAR) studies on a number of novel small molecule

^a Animal Genomics Laboratory, Animal Biotechnology Centre, National Dairy Research Institute, Karnal-132001, Haryana, India. E-mail: ml2mahesh@gmail.com; Fax: +91-1842250042; Tel: +91-1842259503

^b BIF-Centre, Department of Bioinformatics, Orissa University of Agriculture and Technology, Bhubaneswar-751003, Odisha, India

^c Biotechnology Laboratory, Central Inland Fisheries Research Institute, Barrackpore, Kolkata-700120, West Bengal, India. E-mail: jitued@gmail.com

^d Department of Agricultural Biotechnology, Assam Agricultural University, Jorhat-785013, Assam, India

† Electronic supplementary information (ESI) available. See DOI: 10.1039/c4mb00214h

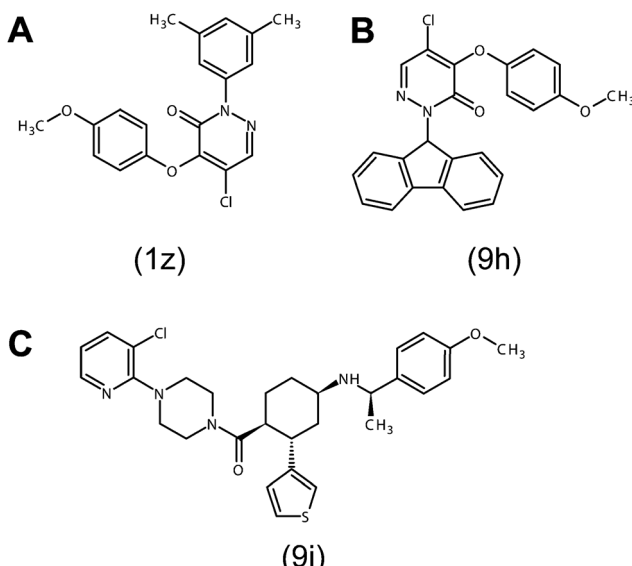


Fig. 1 Chemical structures of antagonists used in this study to explore antagonist binding modes of NPBWR1. (A) 5-Chloro-2-(3,5-dimethylphenyl)-4-(4-methoxyphenoxy)pyridazin-3(2H)-one; **1z**, (B) 5-chloro-2-(9H-fluoren-9-yl)-4-(4-methoxyphenoxy)pyridazin-3(2H)-one; **9h**, (C) [4-(5-chloropyridin-2-yl)piperazin-1-yl][(1S,2S,4R)-4-[(1R)-1-(4-methoxyphenyl)ethyl]amino]-2-(thiophen-3-yl)cyclohexylmethanone; **9i**.

antagonists of NPBWR1. A preliminary SAR analysis of NPBWR1 antagonists had reported the compound [4-(5-chloropyridin-2-yl)-piperazin-1-yl][(1S,2S,4R)-4-[(1R)-1-(4-methoxyphenyl)ethyl]amino]-2-(thiophen-3-yl)cyclohexylmethanone as a lead from a high-throughput screen. This compound showed moderate potency (IC_{50}) of 363 nM and 25 nM in mouse functional and cAMP binding assays, respectively. This lead was further developed into a molecule (designated by the authors as **9i**; Fig. 1A) with picomolar potency in both functional and binding assays.¹² However, **9i** suffered from poor intrinsic metabolic stability (<10% parent remaining at 30 min in mouse liver microsomes). Moreover, it was found to be a substrate for p-glycoprotein that may not specifically bind to NPBWR1. Subsequently, another group reported a novel compound 5-chloro-2-(3,5-dimethylphenyl)-4-(4-methoxyphenoxy)pyridazin-3(2H)-one, designated as **1z**^{CYM50557} (Fig. 1B) with submicromolar antagonist activity ($IC_{50} = 0.27$ mM). **1z** showed high selectivity against a broad range of off-target proteins including GPCRs, enzymes, transporters, and ion channels, but it was found to be poorly soluble in water.¹³ **1z**^{CYM50557} was further optimized into a molecule 5-chloro-2-(9H-fluoren-9-yl)-4-(4-methoxyphenoxy)pyridazin-3(2H)-one (**9h**^{CYM50769}; Fig. 1C) with a submicromolar IC_{50} of 0.12 mM.¹⁴ **9h** was found to be highly specific for a wide range of pharmacologically relevant off-targets and was suggested to be a valuable pharmacological tool to study physiological functions and therapeutic utility of NPBWR1. These successful medicinal chemistry advances encourage further development of innovative antagonists that may provide insights into the atomistic interaction and biological role of the target receptor.

In this study, we constructed a homology model of the NPBWR1 receptor based on the crystal structure of the N/OFQ receptor.

The modeled receptor was refined and optimized in an explicit membrane aqueous environment through molecular dynamics (MD) simulations. The antagonist structures were docked into the predicted receptor binding cavity and the best interacting compound along with the key residues responsible for ligand binding were identified. Molecular Mechanics/Poisson–Boltzmann Surface Area (MM/PBSA) binding free energy calculation and computational alanine scanning (CAS) results established the active site residues responsible for high-affinity antagonist binding. Taken together, we were able to map the active site features crucial for accommodating antagonists within NPBWR1. The results of this study will be useful to study the binding modes of novel agonists and antagonists within the NPBWR1 receptor.

Materials and methods

Homology modeling of NPBWR1

The primary sequence of NPBWR1 (328 amino acids) was obtained from UniProtKB (UniProt ID P48145). The homologous templates were identified using basic local alignment search tool (BLAST)¹⁵ and protein data bank (PDB). The crystal structure of the N/OFQ receptor (PDB ID: 4EA3)¹⁶ with highest identity and lowest *e*-value was considered for constructing the NPBWR1 model. Target-template pair-wise sequence alignment, model building, and loop refinement was carried out in the MODELLER 9.10 program.¹⁷ The discrete optimized potential energy (DOPE) method was implemented to rank the resulting three dimensional (3D) models. The model with the lowest DOPE score was selected for further refinement using energy minimization. The energy minimized model was assessed for stereochemical quality employing Procheck,¹⁸ Verify 3D,¹⁹ ERRAT,²⁰ ProSA,²¹ ProQ,²² and MolProbity²³ web servers.

MD simulation

MD simulation of NPBWR1 was performed using the GROMACS 4.5.5 simulation package²⁴ with a hybrid force field combining “Gromos” and “Berger-Lipid” parameters for protein and lipid atoms, respectively. A pre-equilibrated dipalmitoylphosphatidylcholine (DPPC) bilayer containing 128 lipid molecules was used as the starting structure for the membrane.^{25,26} The overlapping lipids were truncated using InflateGRO methodology.²⁷ Simple point charge (SPC) water molecules were added to the simulation system by increasing the van der Waals (vdW) radius of DPPC lipids up to 0.375 Å to prevent water from entering into the hydrophobic core of the bilayer. The water molecules which strayed into the bilayer core were removed using the Discovery Studio 3.5 (DS 3.5) freeware (Accelrys software Inc., San diego, CA, USA). A physiological ionic strength (0.15 M) of counter ions was added to the system for electroneutrality. Energy minimization was performed without any constraint on the backbone atoms until the maximum force reached 1000 kJ mol⁻¹ nm⁻¹. Electrostatic interactions were calculated by applying the particle mesh Ewald (PME) method and vdW interactions were computed using a cutoff distance of 12 Å. MD simulations were carried out with periodic boundary condition in three stages. First, the NVT ensemble was used for temperature coupling to

323 K with backbone restraints up to 100 ps. Initial random velocities were assigned to the atoms of the molecules according to the Maxwell–Boltzmann algorithm at a temperature of 323 K. Second, the NPT ensemble was used for pressure equilibration with backbone restraints up to 1 ns. Finally, the backbone constraints were removed and the system was allowed to equilibrate up to 30 ns using the Nose–Hoover thermostat coupling scheme. A linear constraints solver algorithm was applied to fix all bonds involving hydrogen atoms. The time step for MD simulation was kept 0.002 ps (2 fs) and snapshots of trajectories were captured at 5 ps time intervals. Trajectory analysis and time-dependent secondary structure prediction were performed using Visual Molecular Dynamics (VMD)²⁸ and GRACE programs [URL <http://plasma-gate.weizmann.ac.il/Grace/>].

Principal component analysis (PCA)

The PCA analysis was performed by constructing a covariance matrix based on the fluctuation of main chain atoms. The matrix was then diagonalized to generate eigenvectors and eigenvalues that describe collective modes of fluctuations of the proteins. For more details on the construction of the covariance matrix and PCA analysis, we suggest referring to this paper.²⁹

Molecular docking

Two dimensional coordinates of the ligands (**9i**, **1z**, and **9h**) were sketched using the chemsketch freeware (<http://www.acdlabs.com/resources/freeware/chemsketch/>) based on the structural formulae given by their discoverers.^{12–14} The initial geometries of the molecules were cleaned and minimized using Automated Topology Builder (ATB) server.³⁰ Each ligand was docked into the binding site of the representative receptor structure obtained from MD simulation using Autodock 4.2.³¹ Structure preparation, grid, and docking parameters were generated using Autodock Tools 1.5.2. Kollman charge was applied for the atom types of NPBWR1, while Gasteiger parameters were set for partial charges of ligand atoms. The active site was identified using the ‘pocket finder’ web server.³² The binding site grid was centered on Asp116^{3,32} (Ballesteros and Weinstein numbering system, described later), located at the middle of transmembrane (TM) III of the receptor with a dimension of $70 \times 70 \times 70$ grid points in X, Y, and Z directions having a grid spacing of 0.375 Å. Lamarckian genetic algorithm and empirical energy functions were used for docking calculation up to 100 iterations. The initial population size was 300 and the maximum number of energy evaluations was 2.5×10^7 . During the docking process, all amino acid residues were kept rigid while the ligands were treated flexible. The docked poses were clustered at a 2.0 Å cutoff root mean square deviation (RMSD) and were ranked according to their binding energy scores.

MD simulation of NPBWR1–antagonist complexes

Three separate MD simulations of 10 ns duration were performed for the lowest energy docked NPBWR1–antagonist complexes. The ligand topologies were generated from ATB server,³⁰ which uses the PM3 method for quantum calculation of the molecular electronic structure.

Binding free energy calculation

A total of 200 snapshots (at a time interval of 5 ps) were extracted from last 2 ns of the 10 ns MD trajectories of NPBWR1–antagonist complexes to calculate the binding free energies. For this purpose, the GMXAPBS tool³³ was used, which implements the MM/PBSA method³⁴ for estimating the binding free energy. The binding free energy is computed according to eqn (1) as follows:

$$\Delta G_{\text{binding}} = G_{\text{complex}} - (G_{\text{protein}} + G_{\text{ligand}}) \quad (1)$$

The calculation of the free energy terms of G_{complex} , G_{protein} , and G_{ligand} is performed as:

$$\langle G \rangle = \langle E_{\text{MM}} \rangle + \langle G_{\text{sol}} \rangle - T\langle S_{\text{MM}} \rangle \quad (2)$$

wherein E_{MM} is molecular mechanics interaction energy, computed as:

$$E_{\text{MM}} = E_{\text{int}} + E_{\text{coul}} + E_{\text{vdW}} \quad (3)$$

wherein E_{int} represents bond, angle, and torsion energies, E_{coul} denotes electrostatic energy, and E_{vdW} stands for vdW energy.

G_{sol} is solvation free energy, which is divided into polar and nonpolar terms:

$$G_{\text{sol}} = G_{\text{polar}} + G_{\text{nonpolar}} \quad (4)$$

Herein, G_{polar} and G_{nonpolar} were estimated using the APBS program.³⁵ The polar contribution, G_{polar} , was calculated by solving the nonlinearized Poisson–Boltzmann equation. The parameters for APBS calculation were as follows: grid spacing, 0.5 Å; temperature, 296 K; and salt concentration, 0.15 M. The nonpolar contribution, G_{nonpolar} , is calculated as:

$$G_{\text{nonpolar}} = \gamma \text{SASA} + \beta \quad (5)$$

where $\gamma = 0.0227 \text{ kJ mol}^{-1} \text{ Å}^{-2}$ and $\beta = 0 \text{ kJ mol}^{-1}$.³⁶ The dielectric boundary was defined with a probe radius of 1.4 Å. In this calculation, the $T\langle S_{\text{MM}} \rangle$ or ΔS_{bind} (conformational entropy) is ignored due to the high computational cost and often inaccuracy of results.

Results and discussion

Overall structure of NPBWR1

The structural features of NPBWR1 and its interaction with the antagonists were studied using a homology-derived model of NPBWR1 solvated in a DPPC membrane and water molecules. The modeled receptor showed a characteristic GPCR-specific tertiary fold with seven TM (7TM) α -helical domains connected by three extracellular (ECL) and three intracellular (ICL) loops (Fig. 2A–C), along with a conserved disulfide bond between TMIII (Cys109) and ECL2 (Cys188), similar to that found in the crystal structure of opioid receptors.^{37–39} In addition, a cytoplasmic helix TMVIII that runs parallel to the membrane surface was noticed, as found in other GPCR structures.^{40–45} Seven GPCR-specific highly conserved amino acids were identified in the NPBWR1 sequence (Fig. 2E and F): Asn55^{1,50} of the GNxxV motif (TMI), Asp83^{2,50} of the LxxxD motif (TMII), Arg134^{3,50} of DRY motif (TMIII/ICL2), Trp163^{4,50} in the middle of TMIV,

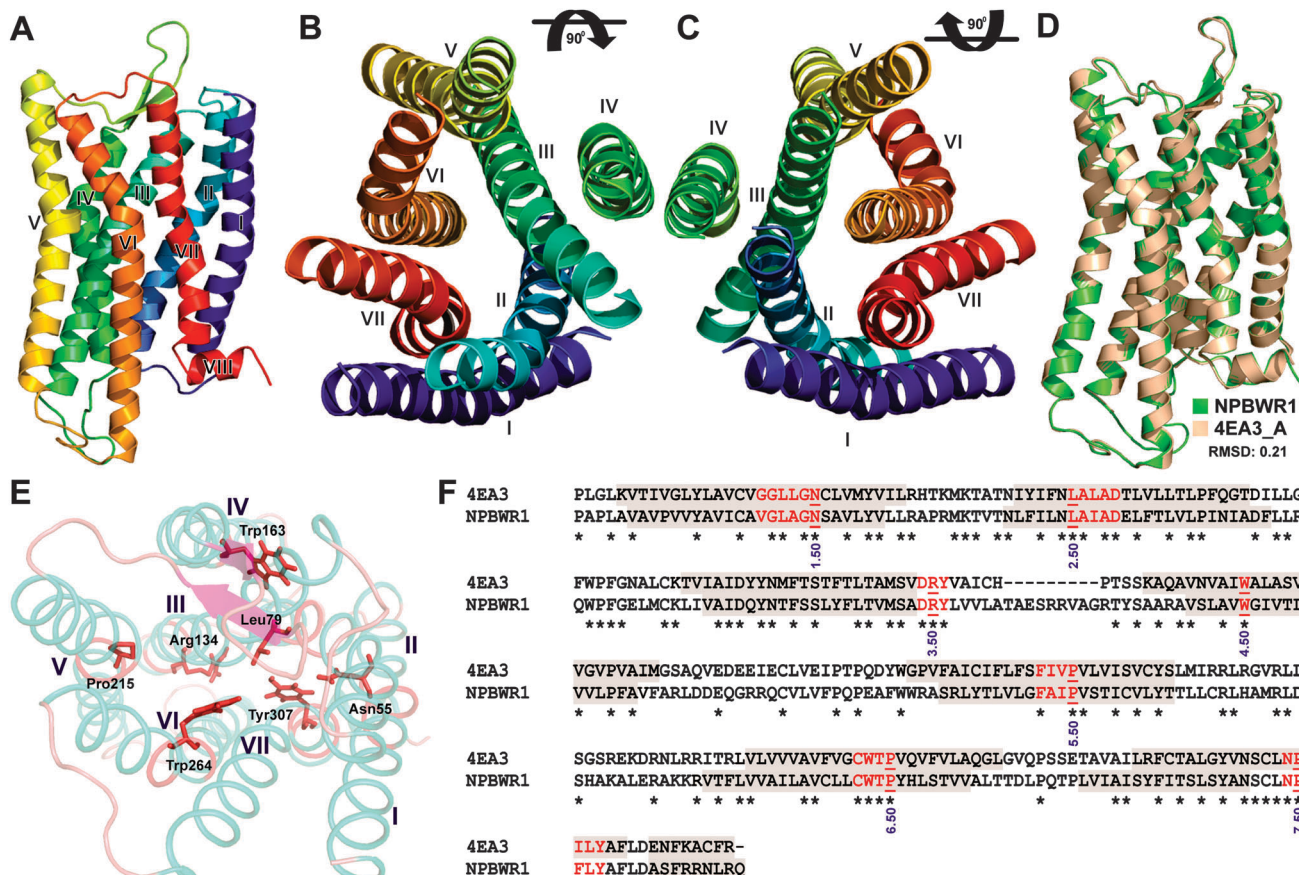


Fig. 2 Overall structural features of modeled NPBWR1 and its comparison with the template NOFQ receptor (PDB ID: 4EA3). (A) The 7TM architecture of NPBWR1 where each helix is colored differently. (B) Top and (C) bottom views of NPBWR1. (D) Structure superimposition of NPBWR1 (green) with 4EA3 (wheat). (E) Structural view of the seven highly conserved GPCR-specific amino acids and their corresponding TM helices. (F) Pair-wise sequence alignment of NPBWR1 and 4EA3, highlighting the TM boundaries (grey shaded), the GPCR-specific signature motifs (red face), and the most conserved residues of each TM helix (underlined), which is labeled by the Ballesteros and Weinstein residue nomenclature (explained in the text).

Pro $215^{5.50}$ of FxxP motif (TMV), Pro $266^{6.50}$ of the CWxP motif (TMVI), Pro 304 of NPxxY motif (TMVII).⁴⁶ These conserved residues are the basis of Ballesteros and Weinstein nomenclature,⁴⁷ which provides a unique two digit identifier to every residue in a GPCR sequence. The first digit represents the helix number and the second digit is the number relative to the most conserved residue of that helix (assigned an index of 50) that increases toward the C-terminus and decreases toward the N-terminus of the index. In this article, the residues of NPBWR1 have been named according to this nomenclature as well as the actual sequence number, for example Asp 116 in TMIII of NPBWR1: Asp $116^{3.32}$. The ECL2 of NPBWR1 and its template N/OFQ receptor¹⁶ were highly similar in terms of sequence and secondary structure (Fig. 2D). The ECL2 retained the canonical β -hairpin architecture, as observed in the crystal structure of opioid receptors (PDB IDs: 4EJ4, 4DKL, 4DJH). The ECL2 is a highly dynamic segment within the GPCR superfamily adopting a secondary structure that depends on the function of the receptor. The solved structures of the β 2-adrenergic receptor (2RH1)⁴⁸ and bovine rhodopsin (1U19)⁴⁹ best illustrate the conformational heterogeneity of ECL2; the former exhibits an open helical ECL2, allowing easy access to larger peptide

hormones into the binding cavity, and the latter exhibits a β -hairpin-like structure that sequesters the receptor binding site from the external milieu.

Analysis of MD trajectory of NPBWR1

MD simulation was performed on the modeled NPBWR1 to better understand the structural changes under dynamic conditions. The overall stability of the model was checked by calculating the RMSD of backbone atoms with respect to their initial positions. The average RMSD of the unliganded inactive receptor model after a 30 ns MD simulation was ~ 3.0 Å (Fig. S1a, ESI†). The model rapidly deviated from its initial conformation during the first 5 ns. This increased backbone deviation could be due to the spontaneous interatomic interactions occurring within the receptor structure as well as between the receptor and the membrane phospholipids and water molecules. After 5 ns, the backbone RMSD kept on oscillating between 2.5 and 3.0 Å up to 15 ns. Afterward, the RMSD reached a stable plateau of 3.0 Å, representing a well equilibrated and satisfactory structural model. The radius of gyration (R_g) is an important measure to monitor the compactness of the receptor TM helices during MD simulation. The average gyration radii of the modeled

NPBWR1 were constant at 21.5 Å (Fig. S1b, ESI†), suggesting a consistent shape and size of the 7TM helical bundle. The root mean square fluctuation (RMSF) of C α atoms was calculated to see the positional fluctuation of individual residues during MD simulation. As seen in Fig. S1c (ESI†), the membrane-bound TM helices were highly rigid showing an average RMSF of <1.0 Å. On the other hand, the ECL and ICL regions showed huge deviation from their initial positions, reaching a RMSF of >3.0 Å. The fluctuations of ECL1 and ICL1 domains were comparatively lower, but the ECL2 deviated up to RMSF = ~4 Å, revealing its highly dynamic nature which is essential for trafficking ligands into the receptor binding cavity. Interestingly, the positional fluctuation of the ECL2 domain decreased substantially during the last 10 ns, indicating a well-equilibrated receptor structure.

Accuracy of the modeled NPBWR1

The accuracy of the optimized model (after MD simulation) was first validated by Ramachandran plot,⁵⁰ which indicated that 99.3% of residues were found in the allowed regions of the plot. Importantly, only 0.8% of residues were found in the disallowed region. The overall G-factor of the built model was 0.09, indicating a good stereochemical quality (Table S1, ESI†). The Verify 3D score was found to be 57.79, which was greater than that of the template, suggesting a good sequence to structure agreement. ERRAT is the overall quality of nonbonded interactions in a protein. The built model showed a score of 97.13, which was higher than the cut-off value of 50%. The Z score of the model, as calculated by ProSA, was highly correlated to that of the template showing a good quality tertiary fold. ProQ analysis revealed that LGscore and MaxSub was 2.46 and 0.18, respectively, indicating an extremely good quality of the model. MolProbit results indicated that the modeled receptor did not show C β deviations, bad backbone bonds and angles within its amino acids. Collectively, all the structure validation parameters were comparable to or higher than those of the template. This indicated that the constructed model could be used for further analysis in this study.

Inactive-state conformation of NPBWR1

The inactive-state conformation of NPBWR1 was constructed based on the crystal structure of the antagonist-bound N/OFQ receptor (sequence identity = 39%). In the inactive-state GPCRs an ionic interaction is assumed between Arg^{3.50} of the D/ERY motif located at the C-terminal end of TMIII and Glu^{6.27} on TMVI. This polar interaction acts as an ‘ionic lock’ that is predicted to stabilize the inactive conformation of the receptor. Agonist induced disruption of this ionic lock causes TMVI to move away from the TM bundle, creating a cleft to dock the heteromeric G protein.^{51,52} However, this ionic lock was broken in the modeled NPBWR1 (Fig. 3A). The reason is that the TMIII–TMVI salt bridge was broken in the template, the N/OFQ receptor, and the fact that Glu243^{6.27} was situated 10 Å away from Arg134^{3.50} in the NPBWR1 model. Evidently, most of the solved structures of antagonist-bound GPCRs lack an ionic interaction between the DRY motif and TMVI. Therefore, a revision of this hypothesis is required until a large number of inactive GPCRs are crystallized having an intrinsic ionic lock.⁵³ Again, it has been reported that Asp133^{3.49} and

Arg134^{3.50} of the DRY motif themselves form a salt bridge interaction in the inactive conformation. Although these two residues were closer to each other in the unliganded NPBWR1 model, their side chain orientations did not favor a polar interaction (Fig. 3A).

Another assumption about GPCR activation is the presence of Trp^{6.48} from the conserved CWxP motif in the middle of TMVI. This Trp^{6.48} (Trp264^{6.48} in NPBWR1), termed ‘toggle switch’, is believed to undergo a side chain rotamerization upon agonist interaction, leading to TMVI movement away from the TM bundle. In the inactive state the rotation of Trp^{6.48} is restricted by neighboring bulky amino acids such as Phe^{5.47} through a π -stacking interaction, termed ‘aromatic lock’. However, this type of interaction was not present in the modeled NPBWR1 receptor (Fig. 3B). We found that Tyr267^{6.51}, His268^{6.52}, and Phe212^{5.47} were situated near Trp264^{6.48}, but these residues were not involved in an apparent ring-stacking interaction with the indole side chain of Trp^{6.48}. The indole ring of Trp264^{6.48} was positioned ‘vertically down’, as observed in most antagonist-bound receptors.^{16,37–39,41,43,45,48,54} It is interesting to note that except for the muscarinic receptor,⁵⁵ no rotameric transition of Trp^{6.48} or its adjacent residues was observed in the active-state GPCRs crystallized so far, even in the prototypical agonist-bound opsin⁵⁶ and β 2-AR⁵⁷ structures.

Tyr^{7.53} of the conserved NPxxY motif, present at the C-terminal end of TMVII, is considered an important activation microswitch in class A GPCRs that exhibits two or three different side chain rotameric states. The outward movement of TMVI during receptor activation is accompanied by a conformational change in Tyr^{7.53} (Tyr307^{7.53} in NPBWR1), which blocks the reverse movement of TMVI. Tyr307^{7.53} displayed a vertically upward side chain orientation in our modeled receptor. All GPCR crystal structures display a highly conserved polar interaction on the inner side of the helical bundle involving the residues of the NPxxY motif. We found a similar type of hydrogen bond (H-bond) network in the NPBWR1 model (Fig. 3C). Asn303^{7.49} of the NPxxY motif was involved in an extended polar interaction network between TMIII, TMII, and TMI. This polar interaction network included Asn55^{1.50}, Asp83^{2.50}, Asn119^{3.35}, Ser123^{3.39}, and Asn299^{7.46}. Among the residues of the polar network, the interaction between Asp83^{2.50} and Asn119^{3.35} corresponds to Asp^{2.50} and Asn^{3.35} of the inactive conformation of the N/OFQ receptor and mutation of this Asp with a Trp resulted in a consistently active receptor without affecting the binding affinity of the endogenous peptide N/OFQ.⁵⁸ The H-bond network in the modeled NPBWR1 gradually became stronger during MD simulation, as indicated by small conformational changes in TMVII, TMIII, TMII, and TMI (Fig. 3D). A minor structural change was recorded for the ECL2 domain during MD simulation where the β -hairpin architecture of ECL2 partially unfolded after 15 ns (Fig. 3E and F), but the conserved disulfide bond between TMIII and ECL2 remained intact throughout the simulation.

Ligand recognition by NPBWR1

The G-protein coupled NPBWR1 is an important receptor that regulates a variety of neuroendocrine functions, such as feeding behavior and energy homeostasis.^{2,3} Malfunction of this

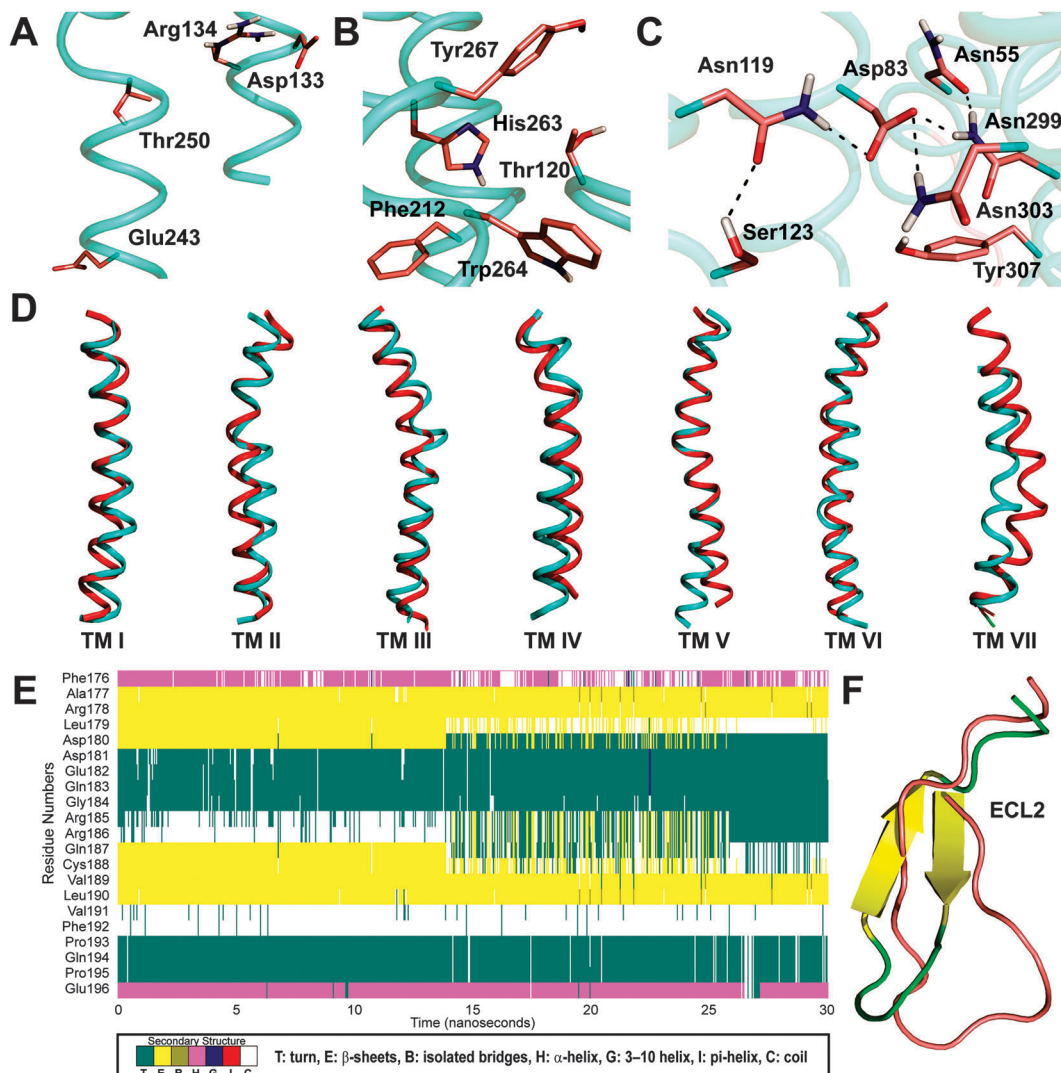


Fig. 3 Schematic diagrams of activation microswitches and secondary structure stability of NPBWR1. (A) Ionic lock. (B) Toggle switch. (C) Conserved polar interaction network. (D) Superimposition of TM helices of initial (cyan) and final (red) NPBWR1 models. (E) Diagrammatic representation of secondary structure fluctuations of ECL2, as calculated using timeline plug-in of the VMD program. The α helices are colored magenta, β sheets are yellow, turns are green, and coils are white. (F) Superimposition of pre and post-MD conformations of ECL2. Yellow colored β sheets indicate the starting conformation.

receptor is associated with sleeping disorder, obesity, and other neuropathic ailments.^{3,59} Despite these facts, limited efforts are being made to develop suitable antagonists for this receptor. Recently, two groups have independently reported some novel antagonistic compounds with varying degrees of affinity toward mouse NPBWR1.^{12–14} However, they did not provide any insight into the binding modes and interactions of these antagonists with NPBWR1. So, to determine the binding site of the antagonists, we first predicted the binding modes between the ligands, **1z**, **9h**, and **9i**, and NPBWR1 through Autodock. Second, the lowest energy complexes selected from each set of docking were subjected to MD simulations and MM/PBSA binding free energy calculations. Third, the receptor-ligand complex showing the lowest binding free energy (highest binding affinity) was chosen for CAS mutations followed by MM/PBSA calculations.

The antagonists docked to NPBWR1 on its surface surrounded by the extracellular ends of TMII, TMIII, TMVI, and TMVII where

they were stabilized by extensive contacts with the three ECL domains, resembling CXCR4.⁴⁵ Table S2 (ESI[†]) shows the docking scores of the three antagonists. The docking energy of the NPBWR1-**9i** complex ($-8.81 \text{ kcal mol}^{-1}$) was a little higher than those of NPBWR1-**1z** ($-8.23 \text{ kcal mol}^{-1}$) and NPBWR1-**9h** ($-8.11 \text{ kcal mol}^{-1}$), suggesting that the strength of interaction of **9i** was a bit stronger than that of **1z** and **9h**. Because **1z** and **9h** do not carry many hydrophilic groups, a slight penalty was found for the electrostatic interactions. Briefly, **1z** was stabilized in the receptor binding cavity by two H-bonds: one with Arg100^{ECL1} and another with Gln187^{ECL2}. **9i** formed a single H-bond with Gln281^{ECL3}. However, **9h** interacted with NPBWR1 mainly through hydrophobic and vdW interactions.

Analysis of intermolecular contacts, after MD simulations, revealed that **9i** was stabilized mainly by electrostatic and vdW interactions. For **1z**, two crucial intermolecular contacts were observed: an aromatic stacking between Trp102^{ECL1} and a

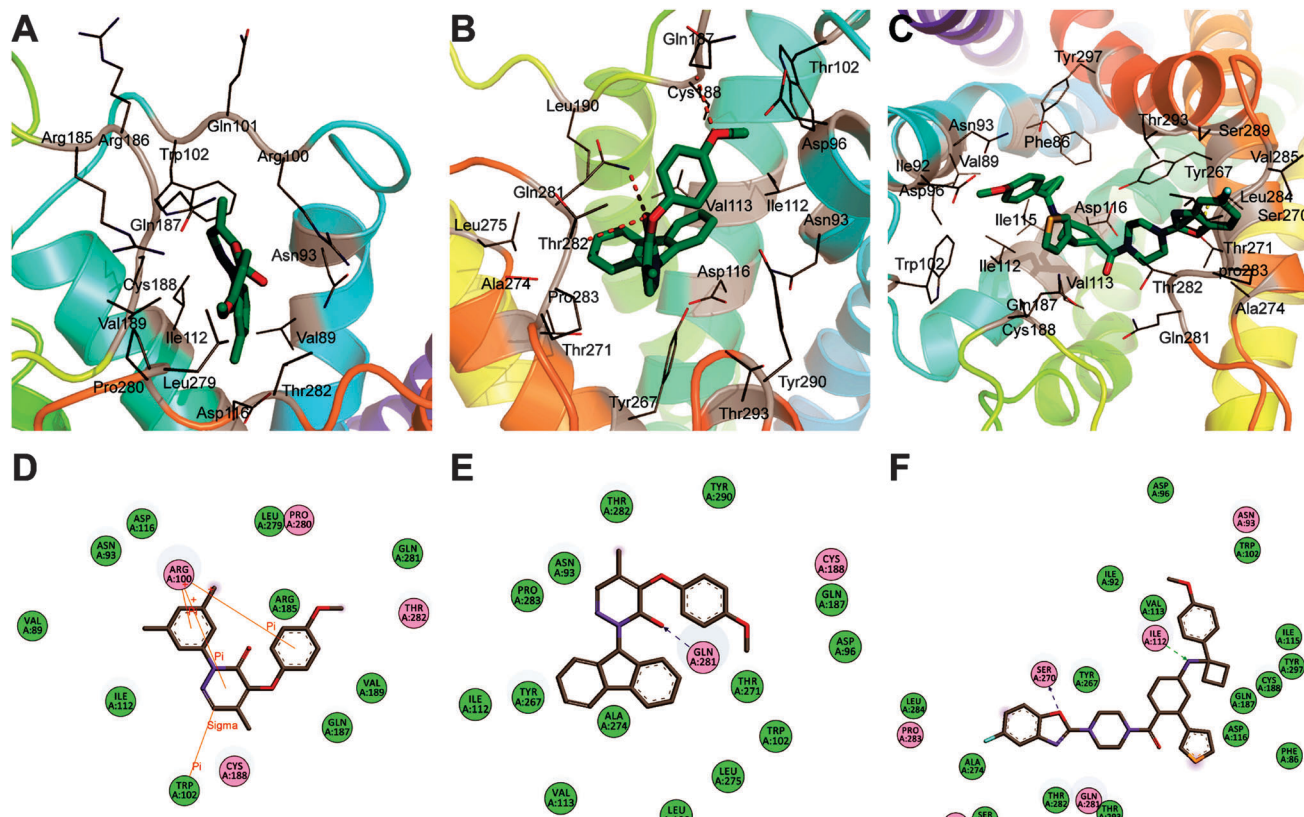


Fig. 4 Schematic diagrams of intermolecular interactions between NPBWR1 and antagonists after 10 ns MD simulation. (A) and (D) Interaction between NPBWR1 and **1z**, (B) and (E) interaction between NPBWR1 and **9h**, (C) and (F) interaction between NPBWR1 and **9i**. H-bonds are indicated by red dashes. The ligands are shown as stick models and the carbon atoms are colored green.

benzyl ring of **1z**; and a cation–π interaction between Arg100^{ECL1} and the methoxybenzyl ring of **1z** (Fig. 4). On the other hand, **9h** was stabilized by a high-affinity H-bond with the side chain amino group of Gln281^{ECL3}. A polar interaction was found between **9h** and Cys188^{ECL2}. Except these two residues, all other residues present around 4 Å of **9h** provided vdW contacts.

The binding free energies between the modeled receptor and the three ligands were calculated using MM/PBSA methods (see Materials and methods). The overall binding free energies of NPBWR1-**1z**, NPBWR1-**9h**, and NPBWR1-**9i** complexes were -217.49 , -263.95 , and -79.18 kJ mol⁻¹, respectively (Table 1). This indicated that **9h** interacted with NPBWR1 more strongly than others, whereas the binding mode between **9i** and NPBWR1 was energetically least stable. The decreased binding affinity of **9i** toward the receptor could be explained by the fact that **9i** was

too big for the binding cavity of NPBWR1. It docked on the receptor surface with an extended conformation where it was seen protruding out from the TM bundle between TMVI and TMVII (Fig. 5A–C). As a result, the TMI and TMVII showed large outward movements away from the TM bundle to avoid steric conflicts between the ligand and the receptor amino acids (Fig. 5F). In contrast, the TM movements of NPBWR1-**1z** and NPBWR1-**9h** complexes were rather similar and were highly restricted (Fig. 5D and E). This was probably because of the structural analogy among **9h** and **1z** (the former is a derivative of the latter) and their similar binding affinities toward the modeled receptor. The obtained binding free energies were decomposed into electrostatic, vdW, polar, and nonpolar solvation free energies (Table 1). It can be seen from Table 1 that the strong binding affinity between the antagonists and the receptor

Table 1 MM/PBSA binding free energy kJ mol⁻¹ decomposition of NPBWR1–antagonist complexes

Conformations	Polar contribution			Non-polar contribution			
	ΔG_{coul}	ΔG_{ps}	ΔG_{polar}	ΔG_{vdW}	ΔG_{nps}	$\Delta G_{\text{nonpolar}}$	ΔG_{bind}
1z	-35.74 (6.1)	125.29 (17.5)	89.55	-289.24 (16.2)	-17.8 (0.4)	-307.04	-217.49 (16.3)
9h	-12.46 (6.9)	124.65 (16.8)	112.18	-354.95 (15.3)	-21.18 (0.5)	-376.14	-263.95 (15.3)
9i	-110.72 (29.2)	275.24 (34.4)	164.51	-216.08 (13.1)	-27.61 (0.4)	-243.7	-79.18 (13.1)

ΔG_{coul} : electrostatic energy. ΔG_{ps} : polar solvation energy. ΔG_{polar} : polar contribution ($\Delta G_{\text{coul}} + \Delta G_{\text{ps}}$). ΔG_{vdW} : van der Waals energy. ΔG_{nps} : nonpolar solvation energy. $\Delta G_{\text{nonpolar}}$: nonpolar contribution ($\Delta G_{\text{vdW}} + \Delta G_{\text{nps}}$). ΔG_{bind} : overall binding free energies. Standard deviations are shown in parentheses.

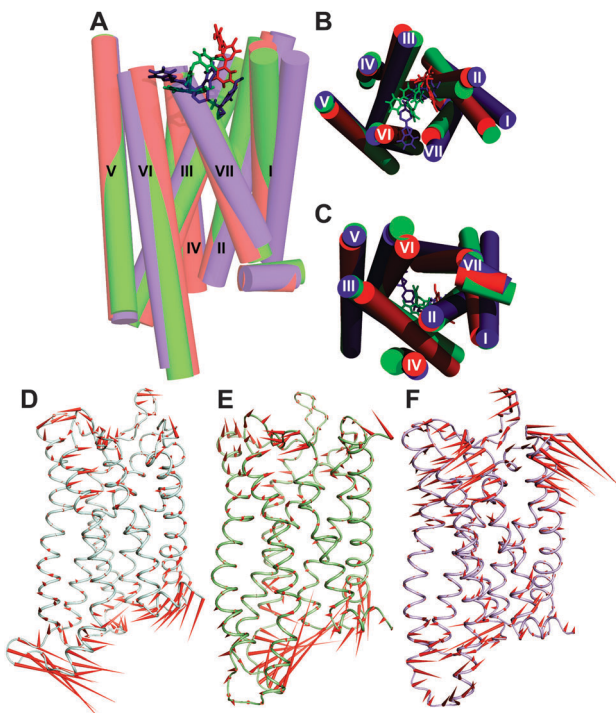


Fig. 5 Antagonist mediated structural movement of TM domains of NPBWR1 (A) superimposition of TM helices of three receptor–ligand complexes; NPBWR1-**1z** (red), NPBWR1-**9h** (green), NPBWR1-**9i** (blue). (B) and (C) Top and bottom views of superimposed NPBWR1–antagonist complexes. (D) to (F) Porcupine plots of NPBWR1-**1z**, NPBWR1-**9h**, and NPBWR1-**9i**, respectively.

was largely governed by the nonpolar terms and that the NPBWR1-**9h** complex had the highest vdW energy. On the other hand, the solute electrostatic free energy of NPBWR1-**9i** was the strongest. The other binding free energy components were comparable in all three complexes, indicating vdW interaction could be pivotal for antagonist recognition in NPBWR1. Taken together, the strength of interaction of **9i** was many times weaker than those of **1z** and **9h**. This observation finds support from the study reporting that **9i** showed poor metabolic stability and it might not bind to the receptor with optimal affinity.¹³ Also, **9i** was found to be a substrate for p-glycoprotein and may not be specific to NPBWR1.¹² Hence **9h** was considered the most suitable ligand for establishing a valid receptor–antagonist model in this study. We performed CAS to identify the essential residues responsible for ligand recognition. To achieve this, we replaced each residue occurring around 4 Å of **9h** with alanine (specifically, Ala274^{6,58} was replaced with Gly). MM/PBSA calculations on each Ala-mutant revealed that the residues Trp102^{ECL1}, Val113^{3,29}, Gln281^{ECL3}, and Ala274^{6,58} were crucial for ligand interaction, since replacement of these residues with simpler amino acids (Ala or Gly) resulted in a loss of binding affinity (Table 2). Our sequence alignment suggested that these residues are evolutionarily conserved throughout the mammalian species (Fig. S2, ESI†).

Antagonist-induced conformational changes in the activation microswitches

Although the ionic lock is believed to be important for stabilizing the inactive state of class A GPCRs, it was broken in the apo as well as holo NPBWR1. However, Asp133^{3,49} and Arg134^{3,50} of

Table 2 MM/PBSA binding free energy kJ mol⁻¹ decomposition of native and Ala-mutant NPBWR1-**9h** complexes

Mutations	Polar contribution			Non-polar contribution			
	ΔG_{coul}	ΔG_{ps}	ΔG_{polar}	ΔG_{vdW}	ΔG_{nps}	$\Delta G_{\text{nonpolar}}$	ΔG_{bind}
9h	-12.46 (6.9)	124.65 (16.8)	112.18	-354.95 (15.3)	-21.18 (0.5)	-376.14	-263.95 (15.3)
Asp96	-5.17 (6.7)	115.77 (17.1)	110.6	-372.66 (17.4)	-21.14 (0.5)	-393.8	-270.59 (18.9)
Trp102	-11.86 (6.9)	122.96 (17.7)	111.1	-353.19 (14.9)	-21.31 (0.5)	-374.5	-250 (16.0)
Asn93	-12.18 (7.0)	127.22 (16.1)	115.04	-356.88 (14.8)	-21.3 (0.5)	-378.19	-263.15 (14.7)
Tyr290	-12.24 (6.8)	118.17 (17.3)	105.92	-350.43 (15.3)	-20.27 (0.4)	-370.71	-264.78 (15.6)
Thr293	-11.96 (7.0)	121.43 (16.8)	109.47	-348.93 (15.3)	-21.12 (0.5)	-370.05	-264.97 (15.4)
Ile292	-12.48 (6.9)	124.43 (17.0)	111.94	-355.17 (15.1)	-21.17 (0.5)	-376.35	-268.39 (15.1)
Gln187	-13.2 (6.9)	123.83 (17.3)	110.63	-355.06 (15.8)	-20.96 (0.5)	-376.12	-269.12 (15.9)
Cys109	-12.37 (7.1)	125.86 (17.2)	113.49	-417.85 (72.1)	-21.18 (0.5)	-439.03	-326.57 (73.0)
Ile119	-12.46 (6.9)	124.65 (16.8)	112.18	-354.95 (15.3)	-21.18 (0.5)	-376.14	-263.95 (15.3)
Cys188	-12.16 (7.0)	124.84 (16.9)	112.67	-415.85 (74.8)	-21.18 (0.5)	-437.04	-325.4 (75.4)
Asp116	-14.78 (6.9)	104.55 (14.8)	89.77	-360.75 (15.7)	-21.15 (0.5)	-381.91	-292.14 (15.7)
Val113	-12.48 (6.9)	124.06 (16.8)	111.58	-344.41 (15.5)	-21.3 (0.5)	-365.71	-254.13 (15.5)
Tyr267	-12.17 (6.8)	109.42 (15.4)	97.25	-338.92 (15.3)	-21.05 (0.5)	-359.98	-262.72 (15.2)
Thr262	-12.46 (6.9)	124.65 (16.8)	112.18	-345.95 (15.3)	-21.18 (0.5)	-376.14	-263.95 (15.3)
Pro283	-12.99 (7.1)	125.40 (16.4)	112.4	-425.59 (72.3)	-21.22 (0.5)	-446.82	-321.79 (73.0)
Gln281	-3.68 (5.2)	113.09 (18.0)	109.4	-341.96 (15.7)	-21.14 (0.5)	-363.11	-256.04 (16.0)
Thr271	-12.9 (7.0)	116.95 (16.2)	104.05	-350.96 (15.4)	-21.14 (0.5)	-372.1	-282.71 (15.3)
Ser270	-11.74 (6.7)	120.29 (16.7)	108.55	-356.59 (14.6)	-21.14 (0.5)	-377.73	-269.18 (14.7)
Ala274 ^a	-12.47 (6.9)	125.34 (17.7)	112.87	-351 (14.7)	-21.25 (0.5)	-372.25	-259.38 (14.7)
Leu275	-12.48 (6.9)	124.88 (17.3)	112.4	-360.55 (15.4)	-21.54 (0.5)	-382.09	-269.68 (15.4)
Leu190	-12.68 (7.0)	124.48 (17.2)	111.79	-353.7 (14.8)	-21.47 (0.5)	-375.18	-263.38 (15.0)
Phe173	-12.65 (6.9)	120.15 (17.7)	107.49	-357.51 (14.2)	-21.25 (0.5)	-278.76	-271.27 (14.4)

^a Ala274 was replaced with Gly. ΔG_{coul} : electrostatic energy. ΔG_{ps} : polar solvation energy. ΔG_{polar} : polar contribution ($\Delta G_{\text{coul}} + \Delta G_{\text{ps}}$). ΔG_{vdW} : van der Waals energy. ΔG_{nps} : nonpolar solvation energy. $\Delta G_{\text{nonpolar}}$: nonpolar contribution ($\Delta G_{\text{vdW}} + \Delta G_{\text{nps}}$). ΔG_{bind} : overall binding free energies. Standard deviations are shown in parentheses.

the DRY motif were found to be involved in a salt bridge interaction in the holo NPBWR1. Arg^{3,50} acts as another activation microswitch, which forms a polar interaction with a Tyr^{5,58} residue from TMV in the active state opsin crystal structure.⁵³ The ionic interaction between Arg134^{3,50} and Asp133^{3,49} also serves as an ‘ionic lock’ to stabilize the inactive conformation of NPBWR1 in the presence of antagonists.⁵⁸ This ionic interaction is not found in the active state GPCRs, for example opsin.⁵⁶ Our analysis of the H-bond and heavy atom distances suggested that this polar interaction equilibrated between formation and breakage in holo NPBWR1, while it remained broken in the apo form. The relative distances between the interacting atoms of Arg134^{3,50} and Asp133^{3,49} during MD simulations of the three receptor-ligand complexes are shown in (Fig. 6). The polar H-bonding network found in the unliganded NPBWR1 was retained in the three receptor ligand complexes, except for NPBWR1-1z where only a single polar contact remained. Tyr307^{7,53} and Asn303^{7,49} of the NPxxY motif formed a polar interaction, which was not found in the apo form.

The rotamer toggle switch is thought to be involved in the activation of class A GPCRs by changing its chi-1 rotamers.

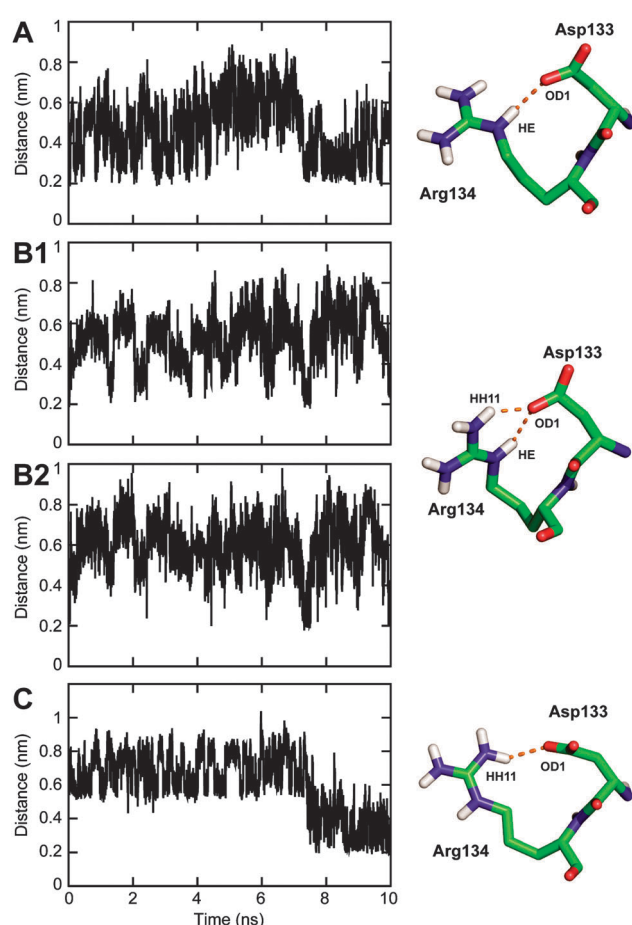


Fig. 6 Distance between interacting atom pairs of the ionic lock (Arg134^{3,50} and Asp133^{3,49}) as a function of simulation time. (A) NPBWR1-1z:Arg134^{3,50}:HE-OD1:Asp133^{3,49} (B) NPBWR1-9h:1, Arg134^{3,50}:HH21-OD1:Asp133^{3,49}, 2, Arg134^{3,50}:HE-OD1:Asp133^{3,49} (C) NPBWR1-9i:Arg134^{3,50}:HH11-OD1:Asp133^{3,49}.

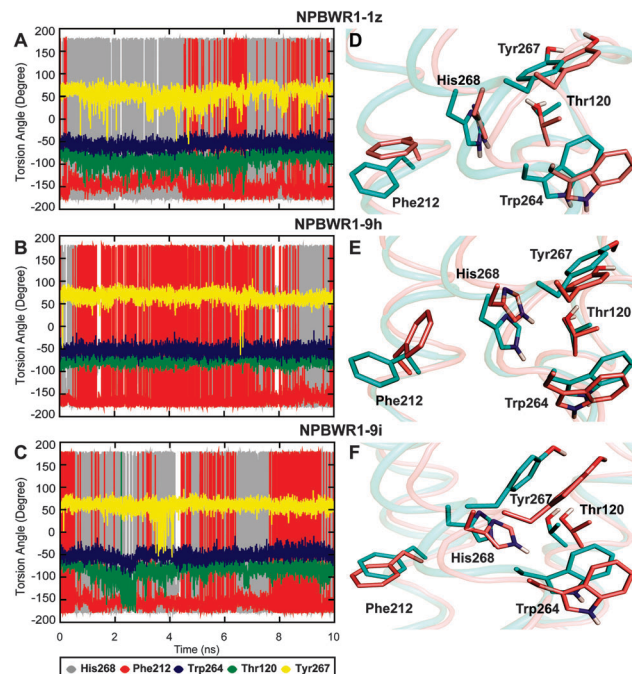


Fig. 7 Measurement of torsion angles (N–C α –C β –C γ) of His268 (grey), Phe212 (red), Trp264 (blue), Thr120 (green), and Tyr267 (yellow) as a function time. (A) NPBWR1-1z, (B) NPBWR1-9h, and (C) NPBWR1-9i. Each panel accompanies a superimposition of pre (cyan) and post-MD (salmon) structures to its right (D–F).

The rotamer toggle switch was composed of Trp264^{6,48} and three other residues, Thr120^{3,36}, His268^{6,52}, Tyr267^{6,51}, which were found to be spatially adjacent to Trp264^{6,48} in NPBWR1. In some GPCRs, a Phe^{5,47} was reported to be involved in a π -stacking interaction with the Trp^{6,48} that restricted its rotation in inactive conformation. But in our case, we did not observe an interaction between Phe212^{5,47} and Trp264^{6,48} in apo as well as in holo receptor models (Fig. 7D–F). We measured the side chain dihedral angles (N–C α –C β –C γ) of Trp264^{6,48}, Thr120^{3,36}, His268^{6,52}, and Tyr267^{6,51} of NPBWR1 to understand the rotameric transitions of these residues during MD simulation in the presence of bound antagonists. The Trp264^{6,48}–Thr120^{3,36}–Tyr267^{6,51} rotamer toggle switch adopted the same rotation states in all three receptor-ligand complexes (Fig. 7A–C), whereas His268^{6,52} and Phe212^{5,47} experienced a chi-1 torsion angle of $\pm 180^\circ$, indicating that these residues did not restrain the rotation of Trp264^{6,48}. The side chain torsion angle of Trp264^{6,48} remained unchanged at $\sim -60^\circ$ in all three receptor-ligand simulation systems with a nearly parallel orientation to TMIII and TMVI, as observed in a previous simulation study with the A_{2A} adenosine receptor.⁶⁰

Conclusion

In conclusion, we modeled a 3D structure of the novel NPBWR1 receptor and studied its ligand binding behavior using three small molecule antagonists, designated as **1z**, **9h**, and **9i**. Molecular docking and MM/PBSA binding free energy calculations

revealed that **9i** had a poor binding affinity for NPBWR1, causing huge conformational alterations in the extracellular surface of the TM bundle. On the other hand, **9h** – a derivative of **1z** – was found to bind to the receptor with high affinity. In the NPBWR1–**9h** complex, the vdW contribution was crucial for the energetic stability of the complex. Furthermore, the GPCR activation related microswitches, such as the ionic lock and toggle switch, were less obvious in the modeled NPBWR1, which is consistent with a number of inactive GPCR crystal structures and modeling studies, suggesting that these activation-related hypotheses require a revision.

References

- B. F. O'Dowd, M. A. Scheideler, T. Nguyen, R. Cheng, J. S. Rasmussen, A. Marchese, R. Zastawny, H. H. Heng, L. C. Tsui, X. Shi, S. Asa, L. Puy and S. R. George, *Genomics*, 1995, **28**, 84–91.
- Y. Shimomura, M. Harada, M. Goto, T. Sugo, Y. Matsumoto, M. Abe, T. Watanabe, T. Asami, C. Kitada, M. Mori, H. Onda and M. Fujino, *J. Biol. Chem.*, 2002, **277**, 35826–35832.
- H. Tanaka, T. Yoshida, N. Miyamoto, T. Motoike, H. Kurosu, K. Shibata, A. Yamanaka, S. C. Williams, J. A. Richardson, N. Tsujino, M. G. Garry, M. R. Lerner, D. S. King, B. F. O'Dowd, T. Sakurai and M. Yanagisawa, *Proc. Natl. Acad. Sci. U. S. A.*, 2003, **100**, 6251–6256.
- V. R. Jackson, S. H. Lin, Z. Wang, H. P. Nothacker and O. Civelli, *J. Comp. Neurol.*, 2006, **497**, 367–383.
- M. Skrzypski, E. Pruszyńska-Oszmałek, M. Ruciński, D. Szczepankiewicz, M. Sasiek, T. Wojciechowicz, P. Kaczmarek, P. A. Kołodziejski, M. Z. Strowski, L. K. Malendowicz and K. W. Nowak, *Regul. Pept.*, 2012, **176**, 51–56.
- Y. Date, M. S. Mondal, H. Kageyama, M. Ghamari-Langroudi, F. Takenoya, H. Yamaguchi, Y. Shimomura, M. Mori, N. Murakami, S. Shioda, R. D. Cone and M. Nakazato, *Endocrinology*, 2010, **151**, 2200–2210.
- M. A. Kelly, C. T. Beuckmann, S. C. Williams, C. M. Sinton, T. Motoike, J. A. Richardson, R. E. Hammer, M. G. Garry and M. Yanagisawa, *Proc. Natl. Acad. Sci. U. S. A.*, 2005, **102**, 9942–9947.
- P. F. Zaratin, A. Quattrini, S. C. Previtali, G. Comi, G. Hervieu and M. A. Scheideler, *Mol. Cell. Neurosci.*, 2005, **28**, 55–63.
- W. K. Samson, J. R. Baker, C. K. Samson, H. W. Samson and M. M. Taylor, *J. Neuroendocrinol.*, 2004, **16**, 842–849.
- B. R. Green, M. Smith, K. L. White, H. S. White and G. Bulaj, *ACS Chem. Neurosci.*, 2011, **2**, 51–66.
- M. Hondo, M. Ishii and T. Sakurai, *Results Probl. Cell Differ.*, 2008, **46**, 239–256.
- R. F. Anthony, N. B. Hastings, R. Moningka, Z. Guo, M. Wang, J. Di Salvo, Y. Lei, D. Trusca, Q. Deng, V. Tong, J. L. Terebetski, R. G. Ball and F. Ujjainwalla, *Bioorg. Med. Chem. Lett.*, 2012, **22**, 1014–1018.
- M. Urbano, M. Guerrero, J. Zhao, S. Velaparthi, S. A. Saldanha, P. Chase, Z. Wang, O. Civelli, P. Hodder, M. T. Schaeffer, S. Brown, H. Rosen and E. Roberts, *Bioorg. Med. Chem. Lett.*, 2012, **22**, 7135–7141.
- M. Guerrero, M. Urbano, M. T. Schaeffer, S. Brown, H. Rosen and E. Roberts, *Bioorg. Med. Chem. Lett.*, 2013, **23**, 614–619.
- S. F. Altschul, W. Gish, W. Miller, E. W. Myers and D. J. Lipman, *J. Mol. Biol.*, 1990, **215**, 403–410.
- A. A. Thompson, W. Liu, E. Chun, V. Katritch, H. Wu, E. Vardy, X. P. Huang, C. Trapella, R. Guerrini, G. Calo, B. L. Roth, V. Cherezov and R. C. Stevens, *Nature*, 2012, **485**, 395–399.
- N. Eswar, B. Webb, M. A. Marti-Renom, M. S. Madhusudhan, D. Eramian, M. Y. Shen, U. Pieper and A. Sali, *Curr. Protoc. Protein Sci.*, 2007, ch. 2, unit 2.9.
- R. A. Laskowski, M. W. MacArthur, D. S. Moss and J. M. Thornton, *J. Appl. Crystallogr.*, 1993, **26**, 283–291.
- R. Lüthy, J. U. Bowie and D. Eisenberg, *Nature*, 1992, **356**, 83–85.
- C. Colovos and T. O. Yeates, *Protein Sci.*, 1993, **2**, 1511–1519.
- M. Wiederstein and M. J. Sippl, *Nucleic Acids Res.*, 2007, **35**, W407–W410.
- B. Wallner and A. Elofsson, *Protein Sci.*, 2003, **12**, 1073–1086.
- V. B. Chen, W. B. Arendall 3rd, J. J. Headd, D. A. Keedy, R. M. Immormino, G. J. Kapral, L. W. Murray, J. S. Richardson and D. C. Richardson, *Acta Crystallogr., Sect. D: Biol. Crystallogr.*, 2010, **66**, 12–21.
- S. Pronk, S. Páll, R. Schulz, P. Larsson, P. Bjelkmar, R. Apostolov, M. R. Shirts, J. C. Smith, P. M. Kasson, D. van der Spoel, B. Hess and E. Lindahl, *Bioinformatics*, 2013, **29**, 845–854.
- M. C. Patra, J. Maharana, S. K. Pradhan and S. N. Rath, *J. Biomol. Struct. Dyn.*, 2014, **32**, 1118–1131.
- M. C. Patra, S. N. Rath, S. K. Pradhan, J. Maharana and S. De, *Eur. Biophys. J.*, 2014, **43**, 35–51.
- C. Kandt, W. L. Ash and D. P. Tieleman, *Methods*, 2007, **41**, 475–488.
- W. Humphrey, A. Dalke and K. Schulten, *J. Mol. Graphics*, 1996, **14**, 33–38.
- A. Amadei, A. B. Linssen and H. J. Berendsen, *Proteins*, 1993, **17**, 412–425.
- A. K. Malde, L. Zuo, M. Breeze, M. Stroet, D. Pogre, P. C. Nair, C. Oostenbrink and A. E. Mark, *J. Chem. Theory Comput.*, 2011, **7**, 4026–4037.
- G. M. Morris, R. Huey, W. Lindstrom, M. F. Sanner, R. K. Belew, D. S. Goodsell and A. J. Olson, *J. Comput. Chem.*, 2009, **30**, 2785–2791.
- M. Hendlich, F. Rippmann and G. Barnickel, *J. Mol. Graphics Modell.*, 1997, **15**, 359–363, 389.
- D. Spiliotopoulos, A. Spitaleri and G. Musco, *PLoS One*, 2012, **7**, e46902.
- I. Massova and P. A. Kollman, *J. Am. Chem. Soc.*, 1999, **121**, 8133–8143.
- N. A. Baker, D. Sept, S. Joseph, M. J. Holst and J. A. McCammon, *Proc. Natl. Acad. Sci. U. S. A.*, 2001, **98**, 10037–10041.
- S. P. Brown and S. W. Muchmore, *J. Med. Chem.*, 2009, **52**, 3159–3165.

- 37 H. Wu, D. Wacker, M. Mileni, V. Katritch, G. W. Han, E. Vardy, W. Liu, A. A. Thompson, X. P. Huang, F. I. Carroll, S. W. Mascarella, R. B. Westkaemper, P. D. Mosier, B. L. Roth, V. Cherezov and R. C. Stevens, *Nature*, 2012, **485**, 327–332.
- 38 A. Manglik, A. C. Kruse, T. S. Kobilka, F. S. Thian, J. M. Mathiesen, R. K. Sunahara, L. Pardo, W. I. Weis, B. K. Kobilka and S. Granier, *Nature*, 2012, **485**, 321–326.
- 39 S. Granier, A. Manglik, A. C. Kruse, T. S. Kobilka, F. S. Thian, W. I. Weis and B. K. Kobilka, *Nature*, 2012, **485**, 400–404.
- 40 V. Cherezov, D. M. Rosenbaum, M. A. Hanson, S. G. Rasmussen, F. S. Thian, T. S. Kobilka, H. J. Choi, P. Kuhn, W. I. Weis, B. K. Kobilka and R. C. Stevens, *Science*, 2007, **318**, 1258–1265.
- 41 V. P. Jaakola, M. T. Griffith, M. A. Hanson, V. Cherezov, E. Y. Chien, J. R. Lane, A. P. Ijzerman and R. C. Stevens, *Science*, 2008, **322**, 1211–1217.
- 42 E. Y. Chien, W. Liu, Q. Zhao, V. Katritch, G. W. Han, M. A. Hanson, L. Shi, A. H. Newman, J. A. Javitch, V. Cherezov and R. C. Stevens, *Science*, 2010, **330**, 1091–1095.
- 43 T. Warne, M. J. Serrano-Vega, J. G. Baker, R. Moukhametzianov, P. C. Edwards, R. Henderson, A. G. Leslie, C. G. Tate and G. F. Schertler, *Nature*, 2008, **454**, 486–491.
- 44 T. Shimamura, M. Shiroishi, S. Weyand, H. Tsujimoto, G. Winter, V. Katritch, R. Abagyan, V. Cherezov, W. Liu, G. W. Han, T. Kobayashi, R. C. Stevens and S. Iwata, *Nature*, 2011, **475**, 65–70.
- 45 B. Wu, E. Y. Chien, C. D. Mol, G. Fenalti, W. Liu, V. Katritch, R. Abagyan, A. Brooun, P. Wells, F. C. Bi, D. J. Hamel, P. Kuhn, T. M. Handel, V. Cherezov and R. C. Stevens, *Science*, 2010, **330**, 1066–1071.
- 46 U. Gether and B. K. Kobilka, *J. Biol. Chem.*, 1998, **273**, 17979–17982.
- 47 J. A. Ballesteros and H. Weinstein, *Methods Neurosci.*, 1995, **25**, 366–428.
- 48 V. Cherezov, D. M. Rosenbaum, M. A. Hanson, S. G. Rasmussen, F. S. Thian, T. S. Kobilka, H. J. Choi, P. Kuhn, W. I. Weis, B. K. Kobilka and R. C. Stevens, *Science*, 2007, **318**, 1258–1265.
- 49 T. Okada, M. Sugihara, A. N. Bondar, M. Elstner, P. Entel and V. Buss, *J. Mol. Biol.*, 2004, **342**, 571–583.
- 50 G. N. Ramachandran, C. Ramakrishnan and V. Sasisekharan, *J. Mol. Biol.*, 1963, **7**, 95–99.
- 51 C. Altenbach, A. K. Kusnetzow, O. P. Ernst, K. P. Hofmann and W. L. Hubbell, *Proc. Natl. Acad. Sci. U. S. A.*, 2008, **105**, 7439–7444.
- 52 X. Yao, C. Parnot, X. Deupi, V. R. Ratnala, G. Swaminath, D. Farrens and B. Kobilka, *Nat. Chem. Biol.*, 2006, **2**, 417–422.
- 53 M. Audet and M. Bouvier, *Cell*, 2012, **151**, 14–23.
- 54 S. G. Rasmussen, H. J. Choi, D. M. Rosenbaum, T. S. Kobilka, F. S. Thian, P. C. Edwards, M. Burghammer, V. R. Ratnala, R. Sanishvili, R. F. Fischetti, G. F. Schertler, W. I. Weis and B. K. Kobilka, *Nature*, 2007, **450**, 383–387.
- 55 A. C. Kruse, A. M. Ring, A. Manglik, J. Hu, K. Hu, K. Eitel, H. Hübner, E. Pardon, C. Valant, P. M. Sexton, A. Christopoulos, C. C. Felder, P. Gmeiner, J. Steyaert, W. I. Weis, K. C. Garcia, J. Wess and B. K. Kobilka, *Nature*, 2013, **504**, 101–106.
- 56 J. H. Park, P. Scheerer, K. P. Hofmann, H. W. Choe and O. P. Ernst, *Nature*, 2008, **454**, 183–187.
- 57 A. M. Ring, A. Manglik, A. C. Kruse, M. D. Enos, W. I. Weis, K. C. Garcia and B. K. Kobilka, *Nature*, 2013, **502**, 575–579.
- 58 P. R. Daga and N. T. Zaveri, *Proteins*, 2012, **80**, 1948–1961.
- 59 N. Hirashima, T. Tsunematsu, K. Ichiki, H. Tanaka, T. S. Kilduff and A. Yamanaka, *Sleep*, 2011, **34**, 31–37.
- 60 X. Pang, M. Yang and K. Han, *Proteins*, 2013, **81**, 1399–1410.